Isoforms of the Erythropoietin receptor in dopaminergic neurons of the *Substantia Nigra*

Marcuzzi, Federica(1); Zucchelli, Silvia(1, 2); Bertuzzi, Maria(1); Santoro, Claudio(2); Tell, Gianluca(3); Carninci, Piero(4); Gustincich, Stefano(1)

(1)Area of Neuroscience, SISSA, Trieste, Italy
(2)Department of Health Sciences, University of Eastern Piedmont, Novara, Italy
(3)Department of Medical and Biological Sciences (DSMB), University of Udine, Udine, Italy
(4)Division of Genomic Technologies, RIKEN Center for Life Science Technologies, Yokohama, Japan

Originally published in: Neurochem. (2016) 139, 596–609

Received June 6, 2016; revised manuscript received July 15, 2016; accepted July 18, 2016.

Address correspondence and reprint requests to Stefano Gustincich, Area of Neuroscience, SISSA, via Bonomea 265, 34136 Trieste, Italy, E-mail: gustinci@sissa.it and Piero Carninci, RIKEN Center for Life Science Technologies, Division of Genomic Technologies, Yokohama Institute, 1-7-22 Suehiro-cho, Tsurumi-ku, Yokohama, Kanagawa 230-0045 Japan. E-mail: carninci@riken.jp

Stefano Gustimcich present address: Department of Neuroscience and Brain Technologies, Italian Institute of Technology, 16163 Genova, Italy

Abbreviations used: CAGE, cap analysis of gene expression; CEPO, carbamylated EPO; EpoR, erythropoietin receptor; LCM, laser capture microdissection; mDA neurons, mesencephalic dopaminergic neurons; Met, methionine; PD, Parkinson's disease; RACE, rapid amplification of cDNA ends; SN, Substantia Nigra; TH, tyrosine hydroxylase; TPM, tag per million; TSS, transcription start site; VTA, ventral tegmental area.

Abstract

Erythropoietin receptor (EpoR) regulates erythrocytes differentiation in blood. In the brain, EpoR has been shown to protect several neuronal cell types from cell death, including the A9 dopaminergic neurons (DA) of the *Substantia Nigra* (SN). These cells form the nigrostriatal pathway and are devoted to the control of postural reflexes and voluntary movements. Selective degeneration of A9 DA neurons leads to Parkinson's disease. By the use of nanoCAGE, a technology that allows the identification of Transcription Start Sites (TSSs) at a genome-wide level, we have described the promoter-level expression atlas of mouse A9 DA neurons purified with Laser Capture Microdissection (LCM). Here, we identify mRNA variants of the Erythropoietin Receptor (DA-EpoR) transcribed from alternative TSSs. Experimental validation and full-length cDNA cloning is integrated with gene expression analysis in the FANTOM5 database. In DA neurons, the EpoR gene encodes for a N-terminal truncated receptor. Based on STAT5 phosphorylation assays, we show that the new variant of N-terminally truncated EpoR acts as decoy when co-expressed with the full-length form. A similar isoform is also found in human. This work highlights new complexities in the regulation of Erythropoietin (EPO) signaling in the brain.

Keywords: dopaminergic neurons, erythropoietin, erythropoietin receptor, Parkinson's disease.

EpoR is an highly conserved member of the cytokine receptor super-family, whose activation is triggered by dimerization induced by EPO (Bazan 1989; Constantinescu et al. 1999; Livnah *et al.* 1996; Schneider *et al.* 1997; Yu *et al.* 2001). Since EpoR does not possesses endogenous tyrosine kinase activity, EPO binding initiates the phosphorylation of numerous receptor-associated proteins (Witthuhn et al. 1993) and in turn activates Janus kinase (JAK/STAT)-, Ras/MAP (Ras protein/mitogen-activated protein) kinase-, phosphatidylinositol-3 kinase (PI-3 kinase)- as well as protein kinase C-dependent pathways. The receptor–ligand complex is then internalized and degraded, while signaling pathways are terminated by dephosphorylation of EpoR and JAK-2 (Klingmuller et al. 1995).

EpoR structure and function has been of great interest for the fundamental role of EPO in erythrocytes differentiation in the blood and the consequent use of recombinant hEPO as standard of care for treatment of anemia.

Recently, it has become evident that the EPO/EpoR system presents a broad range of non-hematopoietic effects (Dame et al. 2001). Functional EpoRs have been found in non-erythroid blood cell lines, as lymphocytes, myeloid cells, and megakaryocytes. Furthermore, EpoR is abundantly expressed in the embryonic, fetal, and adult central nervous system (Marti et al. 1996). EpoR immunoreactivity has been found in the somata and proximal dendrites of neurons as well as in astrocytes and choroid plexus (Juul et al. 1998). While liver and kidney are the major site for production of EPO in fetal and adult organisms, biologically active EPO is also synthesized in the brain by selective types of neurons and glial cells having important roles in the neurodevelopment and in modulation of neurotransmission (Digicaylioglu et al. 1995; Masuda et al. 1994). Administration of recombinant EPO to the brain improves learning and memory (Vogel and Gassmann 2011) and is neuroprotective against cell death induced by excitotoxicity, cerebral ischemia, and traumatic injury (Brines et al. 2000; Chong et al. 2003; Digicaylioglu and Lipton 2001; Kawakami et al. 2001; Siren et al. 2001). EPO may also stimulate neurogenesis and exert anti-inflammatory effects. All these features have suggested EPO as potential therapeutics for neurodegenerative diseases (Merelli et al. 2015; Tsai et al. 2006). Importantly, EPO displays trophic effects on A9 DA neurons of the Substantia Nigra (SN), the cells that degenerate in Parkinson's disease (PD). In vitro EPO promotes growth and differentiation of cultured DA cells, while in vivo, it may trigger striatal dopamine release (Lee et al. 2003; Yamamoto et al. 2000). Furthermore, EPO protects A9 DA cells from neurochemical intoxication in PD models in vitro and in vivo (Erbas et al. 2015; Ganser et al. 2010; Jia et al. 2014; Qi et al. 2014; Signore et al. 2006; Xue et al. 2010, 2007). These data has led to first-stage PD clinical trials in human (Jang et al. 2014; Pedroso et al. 2012).

Cap analysis of gene expression (CAGE) is based on sequencing the $5^{\prime}$ extremity of capped RNAs (sequence tags) and allows the precise mapping of transcription start sites (TSS)s (Shiraki et al. 2003). Moreover, the number of sequence tags is proportional to the quantity of RNA in the cell or tissue of origin. Therefore, CAGE provides a qualitative and quantitative map of promoter activities genome-wide (Carninci et al. 2006; Gustincich et al. 2003). More recently, the FANTOM5 project has developed a modified protocol for high-throughput single molecule CAGE sequencing with Helicos (hCAGE). hCAGE has been applied to a wide range of human and mouse cell lines, primary cells and tissues, thus providing an unprecedented dataset of promoter usage (Forrest et al. 2014). Since CAGE typically requires a relatively large amount of starting material, we recently developed a miniaturized version of CAGE technology, that we named nanoCAGE for its requirement of just few nanograms of RNA (Plessy et al. 2010). NanoCAGE has been recently applied to identify active TSSs in mouse olfactory epithelium (OE) (Plessy et al. 2012).

To gain insights into A9 DA cell physiology, we performed nanoCAGE analysis on isolated Green Fluorescent Protein (GFP)-labeled neurons. By this experimental approach, we have previously shown that A9 neurons express a repertoire of olfactory receptors (Grison et al. 2014). Most importantly, we proved that they selectively expressed alpha and beta chains of hemoglobin, a protein previously thought to be present exclusively in the red blood cells (Biagioli et al. 2009).

In this work, we precisely map TSS distribution at EpoR gene locus in DA cells and extend this analysis to FANTOM5 dataset, proving that both mouse and human EpoR genes synthesize an N-terminal truncated isoform that acts as decoy for EPO signaling.

Methods

Bioinformatic analysis

Analysis of FANTOM5 promoter-level expression atlas was performed with publicly available datasets (http://fan-tom.gsc.riken.jp/5/) (Andersson et al. 2014; Arner et al. 2015; Forrest et al. 2014) and the Zenbu genome browser tool (Severin et al. 2014). Expression values were extracted with specific tools available on web-based Zenbu interface.

Animals

All the experiments involving the use of animals were performed following permissions from SISSA Ethical Committee and in accordance with European guidelines for animal care. C57BL/6J (Harlan Laboratories, S.R.L., Italy) were obtained from SISSA Animal Facility. TH-GFP/21-31 transgenic mice, courtesy of Matsushita et al. (2002), were maintained in heterozygosity by breeding to C57BL/6J mice in SISSA Animal Facility.

Laser capture microdissection (LCM) and tissue preparation

LCM and pressure catapulting were used to harvest A9 neurons after fixation with a zinc-fix-based method that assured the preservation of both tissue morphology and RNA integrity. RNA was then used as a template for nanoCAGE gene expression analysis. LCM was performed on 8–12 weeks old female TH-GFP/21-31 mice as previously described (Biagioli et al. 2009; Carrieri et al. 2012, 2015). C57BL/6J female mice (12 weeks old) were used for in situ hybridization and immunohistochemistry experiments. Intracardiac perfusions were done under total anesthesia.

For RNA and protein assays, tissues (spleen, ventral midbrain, and liver) were dissected from age- and sex-matched animals and immediately put in liquid nitrogen, stored at 80°C, and subsequently processed.

For preparation of membranes from mouse tissues, spleen and ventral midbrain were dissected and homogenized. Membrane preparation was performed using Qproteome cell compartment kit (Qiagen, Valencia, CA, USA) according to manufacturer's instruction.

RNA purification, RT-PCR, and RACE

Total RNA was extracted from mouse tissues using Trizol reagent (Invitrogen, Carlsbad, CA, USA) and purified on RNAeasy columns (Qiagen). RNA quality was tested on denaturing formaldehyde gels. RNA was extracted from LCM-purified neurons using Absolutely Nanoprep kit (Stratagene, La Jolla, CA, USA) according to manufacturer's instructions and eluted in 12 lL volume. RNA quality and yield was analyzed with RNA6000 Pico Lab Chips (Agilent technologies, Palo Alto, CA, USA). All purified RNA samples were treated with DNase I (Ambion, Austin, TX, USA). Reverse transcription was performed with SuperScript III (Invitrogen). Non-quantitative PCR was done using ex-Taq (Takara, Ohtsu, Japan) and following standard protocols.

Rapid amplification of cDNA ends (RACE) was performed with GeneRacer kit (Invitrogen), using purified RNA from mouse tissues and LCM-collected cells. All RACE reactions were carried out with nested PCR using Platinum

Taq High Fidelity (Invitrogen). All PCR products were cloned into pGEM-T easy vector system and sequenced (IGA sequencing facility, Udine, Italy).

List of primers used for PCR and RACE experiments are provided in Table 1.

Table 1. List of primers of PCR and RACE

Mouse EpoR	
5′RACE PRIMERS	
GENERACER 5′ PRIMER	CGACTGGAGCACGAGGACACTGA
GENERACER 5^0 NESTED primer	GGACACTGACATGGACTGAAGGAGTA
5′ RACE REV	ATAGCGAGGAGAACCGGACGCCTCC
5′ RACE REV nested	ACTCGATGTTGTCCGCTGTTGGCAGTGAA
3′RACE PRIMERS GENERACER	GCTGTCAACGATACGCTACGTAACG
3′PRIMER GENERACER	CGCTACGTAACGGCATGACAGTG
3′NESTED primer	
3′RACE EPOR5 FW	AGGAAATGAGAGAAATGCTTACAC
3′RACE EPOR6 FW	CATTCTGGTCCTCATCTCGCTGTTG
SCREENING 3^0	
FW EXON1 EPOR	TGACCCAGCTGTGGACTAGGGGAAA
FW EXON TAG	GAAGACTTGGTGTGTTTCTGGGAGGA
EPOR	
REV EXON1	GGAGGCTGGGTGAAGGTGCCC
REV EXON2	ATGAGAAGCTGTAGTTGAAGTCCATCC
REV EXON3	TTCATATCGGATGTGGGTGGTCATAG
REV EXON4	AGTTACCCTTGTGGGGTGGTGAAGA
REV EXON5	CTCAGACCAGGCACTCCAGAAT
REV EXON6	CAACAGCGAGATGAGGACCAGAATG
REV EXON7	GATATGGATGATGCGGTGATAGCGA
REV EXON8	GAGTCCTAGGAGCAGGCCACATAG
Human EPOR	
hEpoR FW1	ATGGACCACCTCGGGGCGTC
hEpoR Rev1	CTTTGCTCTCGAACTTGGGGTCCGG
hEpoR Fw2	CCGAAGAGCTTCTGTGCTTCACCGAG
hEpoR Rev2	TCGAGCTGGTAGGAGAAGCTGTAGTTGC
hEpoR Fw3	GATGAGCCATGGAAGCTGTGTCGC
hEpoR Rev3	GGATGACACGGTGATATCGCGGAGC
hEpoR Fw4	TGACGAGAGCGGCCACGTAGTG
hEpoR Rev4	CTGTACGCTCCCTGCGCCGTTG
hEpoR Fw5	ATGGCTGAGCCGAGCTTCGGCG
hEpoR Rev5	CAGCGACACAGGCTCCGACCAG
hEpoR Fw6	ACCTGGACCCCCTCATCCTGACG
hEpoR Rev6	AGAGCAGCGCGAGCACGGTC
hEpoR Fw7	CTGAAGCAGAAGATCTGGCCTGGCATC

hEpoR Rev7	GGAAGTTACCCTTGTGGGTGGTGAAGA
hEpoR Fw8	CTGTGGCTGTACCAGAATGATGGCTGC
hEpoR Rev8	CTAAGAGCAAGCCACATAGCTGGG
RACE PRIMERS	
hEpoR RACE 2	GTAGGAGAAGCTGTAGTTGCCCGGGCC
hEpoR RACE nest2a	GCGCTCGCCGCTTCCTCCCAGAAACAC
hEpoR RACE nest2b	ACCAAGTCCTCCAACCGCTCGGTGAAGC
hEpoR RACE 7	GAAGTTACCCTTGTGGGTGGTGAAGAGGCC
hEpoR RACE nest7	GGGCTCGGGATGCCAGGCCAGATCTTC
hEpoR RACE nest6	GTGGGAGAGCAGCGCGAGCACGGTC

In situ hybridization

Locked nucleic acid (LNA) DNA probes targeting EpoR exon1 and exon3 were designed using LNA Oligo Optimizer Tool and purchased from Exiqon. In situ hybridization with LNA probes was performed as previously described (Obernosterer et al. 2007). Briefly, after perfusion with 4% paraformaldehyde in Tris-buffered saline (TBS), mouse brain was removed, post-fixed, and cryoprotected overnight at 4°C in 30% sucrose. In situ hybridization was performed on cryostat slices (16 µm) incubating LNA probes at 250 nM at 55°C for 16 h. Signal from LNA probes was detected with anti-DIG antibody (Sigma-Aldrich, St. Louis, MO, USA). DA neurons were visualized by immunofluorescence upon incubation with anti-TH antibody (1 : 1000; Chemicon, Temecula, CA, USA). Fluorescent dye-conjugated secondary antibodies (goat anti-rabbit 594 and goat anti-mouse 488) were used for visualization. Sections were washed, mounted with Vectashield (Vector Laboratories, Burlingame, CA, USA) mounting medium, and observed at confocal microscope (LEICA TCS SP2).

Cloning

FL-EpoR: Full-length cDNA sequence for full-length EpoR (NM_010149) was amplified from spleen by PCR with the following primers:

For EpoR exon1: $5^{\prime}$-TGACCCAGCTGTGGACTAGGGGAAA-$3^{\prime}$

Rev EpoR exon8: $5^{\prime}$-GAGTCCTAGGAGCAGGCCACATAG-$3^{\prime}$

DA-EpoR: DA isoform was cloned from LCM-purified A9 neurons by PCR with the following primers:

For EpoR TSS race: $5^{\prime}$-GAAGACTTGGTGTGTTTCTGGGA GGA-$3^{\prime}$

Rev EpoR exon8: $5^{\prime}$-GAGTCCTAGGAGCAGGCCACATAG-3^{0} PCR products were inserted into pGEM-T-easy vector and sequence verified. For expression analysis in the mammalian cells, FL-EpoR and DA-EpoR were subcloned into pCDNA3.1(-) using EcoRI restriction site.

Cell culture

Human embryonic kidney 293T (HEK 293T) cells were grown in Dulbecco's modified Eagle's medium (GIBCO) supplemented with 10% fetal bovine serum (Sigma-Aldrich, St. Louis, MO, USA), 100 IU/mL penicillin, and 100 lm/mL streptomycin (Sigma-Aldrich, St. Louis, MO, USA) at 37°C in a humidified CO_2 incubator.

MN9D-Nurr1Tet-On cells (Hermanson et al. 2003) were kindly provided by professor T. Perlmann (Ludwig Institute for Cancer Research, Stockholm, Sweden). Cells were maintained in Dulbecco's modified Eagle's medium/F12 medium (Invitrogen) supplemented with 10% fetal bovine serum, in the presence of penicillin (50 units/ mL), streptomycin (50 units/mL), and 250 mM neomycin. Nurr1 expression was induced by 3 µg/mL doxycycline hyclate (Sigma).

Transfection was performed with Lipofectaime 2000 (Invitrogen) following manufacturer's instructions.

For receptor activation, transfected HEK 293T cells were treated with 5 U/mL EPO (R&D Systems, Inc., Minneapolis, MN, USA). Cell lysates were prepared in 29 Laemlli buffer, boiled, and analyzed by western blot.

Western blot

For western blot, samples were resolved on 10% and 12% sodium dodecyl sulfate–polyacrylamide gel electrophoresis, and proteins were transferred to nitrocellulose membrane (Schleicher&Schuell, Florham Park, NJ, USA). Membrane was blocked with 5% non-fat milk in Tris-buffered saline solution (TBST), then incubated overnight at 4°C with the following primary antibodies: anti-b-actin 1 : 5000 (A5441, Sigma), anti-EpoR N-term (W-20) and C-term (M20) (Santa Cruz Biotechnology, Santa Cruz, CA, USA), anti-GFP rabbit polyclonal antibody 1 : 1000 (Cat. No. A6445; Life Techologies, Thermo Fisher Scientific, Waltham, MA, USA), anti-pSTAT5 1 : 1000 (#9351; Cell Signaling). Proteins were detected with the appropriate horseradish peroxidase-conjugated secondary antibodies (DakoCytomation, Glostrup, Denmark) and Enhanced chemiluminescence reagents (Amersham Pharmacia Biosciences).

Immunohistochemistry and immunocytochemistry

Immunohistochemistry was performed as previously described (Biagioli et al. 2009; Carrieri et al. 2012; Grison et al. 2014) on 16-lm-thick cryoslices prepared from 12 weeks old C57BL/6J mice. Primary antibodies targeting N-term (anti-EpoR W-20) and C-term (anti-EpoR M20) of EpoR (Santa Cruz Biotechnologies) were used. DA neurons were identified with anti-TH antibody 1 : 1000 (Chemicon). Immunocytochemistry experiments were performed on transfected HEK 293T cells following a non-permeabilization protocol as previously described (Grison et al. 2014). Cells were incubated with C-terminally targeted anti-EpoR M-20 antibody (Santa Cruz Biotechnology). All images were collected using a confocal microscope (LEICA TCS SP2).

Post-mortem human brain samples

Brain samples were obtained from the Bio-Bank of the Institute of Neuropathology HUB-ICO-IDIBELL (University Hospital of Bellvitge- IDIBELL Foundation), following the guidelines of Spanish legislation on this matter and in compliance with the Helsinki Declaration. Samples were dissected at autopsy with the informed consent of patients or their relatives and the institutional approval of the local Ethics Committee (HUB-ICO/CEIC). SN and cortex were dissected at the time of autopsy, and immediately frozen and stored at 80°C until use. RNA and proteins were extracted using Trizol reagent.

Data access

NanoCAGE sequences from A9 and A10 DA neurons have been submitted to the DNA DataBank of Japan Sequence Read Archive under accession number DRA000475. Data will be available upon release of an accompanying manuscript (Lazarevic et al., submitted). Genomic tools and data downloads from the FANTOM5 project are summarized here http://fantom.gsc.riken.jp/5/.

Statistical analysis

When required, we performed statistical analysis using Excel software. Data were obtained from $n \geq 3$ replicas. Statistically significant differences were assessed by Student's t-test.

Results

Identification of alternative TSSs for EpoR in A9 DA neurons

To study the physiology of A9 DA neurons, we revealed their expression profiles with nanoCAGE (Plessy et al. 2010) on LCM-isolated fluorescently labeled cells (Biagioli et al. 2009). Purified RNA was used for transcriptome analysis. The complete description of A9 transcriptional landscape will be presented elsewhere (Lazarevic D., et al., submitted).

With nanoCAGE, we can annotate sequenced tags to the reference mouse genome, thus identifying TSS and promoter regions in DA cells.

Here, we analyzed TSS usage in the EpoR gene. The full-length transcript for mouse EpoR (FL-EpoR) is localized on chromosome 9 and comprises 8 exons. While the canonical ATG is located in exon 1, exons 1-5 encode the extracellular ligand-binding region, exon 6 the transmembrane domain, and exons 7-8 the cytoplasmic C-terminal of the protein.

As shown in Fig. 1, nanoCAGE tags mapping showed A9 neurons present alternative TSSs for EpoR. In detail, we identified three different TSSs: two intronic, mapping in the first and fifth introns, and one located on the second exon. We named the two alternative transcripts originated from 5^{I} ends in first intron and second exon as DA-EpoRs.

TSSs usage at EpoR locus in mouse tissues and cells

To gather a broader view of DA-EpoR expression, we interrogated FANTOM5 mouse datasets, including almost 1000 libraries from various cells and tissues (Arner et al. 2015; Forrest et al. 2014). To identify genome-wide promoter usage, the FANTOM5 consortium developed decomposition-based peak identification method. For EpoR analysis, high reliable promoters were defined as 'robust' by applying tag evidence thresholds. Expression is therefore based on Relative Log Expression (RLE) normalized values, filtered for 3 tags/library, and measured as tag per million (TPM) (Forrest et al. 2014). We visualized TSSs using the publicly available FANTOM5 Zenbu Genome Browser tool (Severin et al. 2014). For our analysis, we interrogated all hCAGE libraries pooled together and then we focused our attention on spleen and primary neurons derived from SN. Two major transcript variants exist, derived from major promoter1 (p1) and two minor 'robust' promoters, both expressed in red blood cells-derived libraries (Fig. 1).

p1 supports the expression of FL-EpoR as highly enriched in spleen, fetal liver, and erythropoietin-stimulated J2E erythroblastoid cells. Alternative EpoR TSSs identify two minor promoters p@chr9_21766785 and p@chr9_21766830 that are located in the first intron. They are always expressed at lower levels than p1. Libraries from primary neurons derived from SN are included in mouse FANTOM5 collection, although no separation among different mesencephalic DA neurons is present. When lower thresholds for promoter identification are applied, the presence of 'permissive' promoters is evident in SN neurons giving rise to additional variants of EpoR. Among these, TSSs are positioned in the first intron and in the second exon few base pairs aside from the TSSs of DA-EpoR confirming their existence with an independent technology. Expression of alternative EpoR variants can also be measured in different brain regions, as cerebellum, cortex, hippocampus, and striatum.

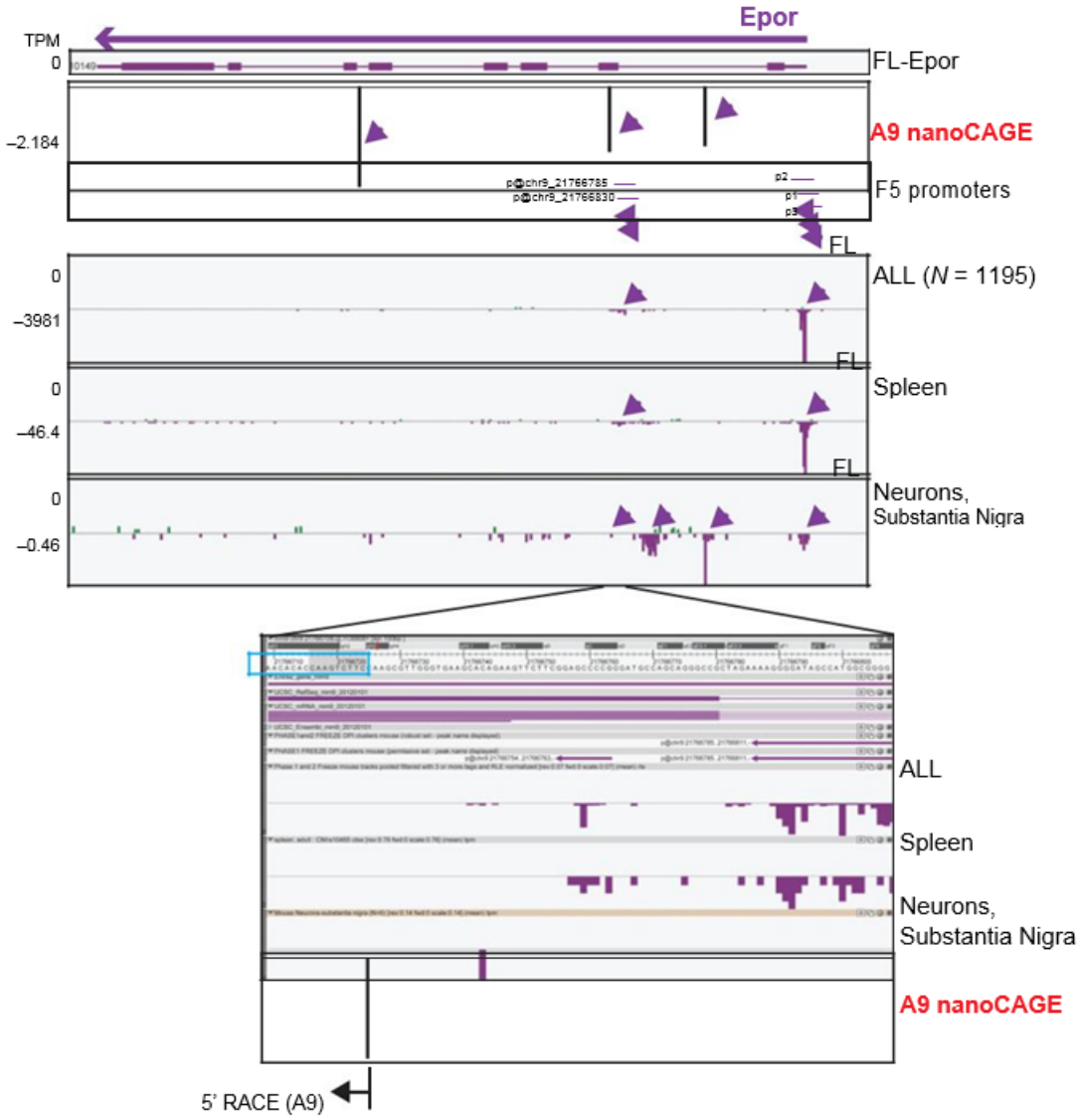

Fig. 1 Transcription start site (TSS) identification in A9 DA cells and in mouse tissues. Zenbu Genome Browser view of mouse Epor locus. Data from A9 nanoCAGE analysis (in red) are imported into Zenbu browser for visualization and comparison with FANTOM5 hCAGE data. EpoR gene (purple arrow) and anatomy of full-length transcript are shown on top. hCAGE data are presented for all libraries pooled together (ALL, n = 1195) and for tissues/cells of interest (spleen, SN primary neurons). Purple arrows highlight alternative Epor TSSs identified by nanoCAGE and FANTOM5 (p1, p2, and p3, p@chr9_21766785 and p@chr9_21766830, in $5^{\prime}$ to $3^{\prime}$ orientation relative to Epor). TSS supporting the expression of full-length Epor transcript in spleen and SN neurons is also indicated. Promoters identified with FANTOM5 decomposition-based peak identification method are shown (original promoter nomenclature is given). A zoomed-in image of the genomic region around the first intron or second exon boundary is provided. A black arrow indicates the position of $5^{\prime}$ rapid amplification of cDNA ends (RACE) results from isolated A9 DA neurons. The validated sequence is highlighted by a blue box.

Validation of the expression of alternative EpoR transcripts in A9 DA cells and characterization of their molecular anatomy

To validate the existence of $5^{\prime}$ end variants of EpoR with an independent technology, we carried out $5^{\prime}$ RACE from 5000 isolated A9 DA neurons. As control, $5^{\prime}$ RACE was carried out on total RNA extracted from spleen, in which FL-EpoR, the canonical form of EpoR, is expressed at high levels. After the ligation of a synthetic RNA oligonucleotide to the 5^{0} end of decapped RNA and retrotranscription, first-step RT-PCR was carried out using the GeneRacer™ $5^{\prime}$ primer and a reverse primer located to the third exon. Nested RT-PCR gave rise to a 500 bp long PCR product from spleen (as expected for a full-length transcript) and a fragment of smaller size (200 bp) from A9 DA neurons (DA-EpoR) (Fig. 2a). Sequencing confirmed nanoCAGE TSS identification at 280 bp $3^{\prime}$ to the canonical sequence and localized in the second exon of the EpoR gene.

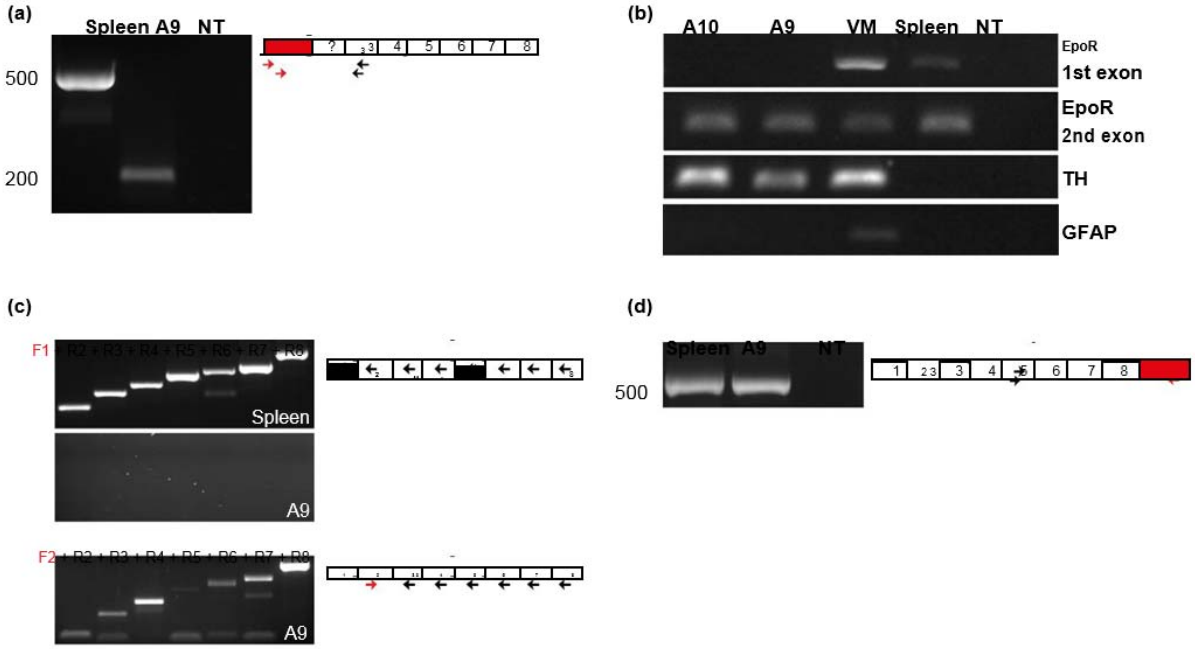

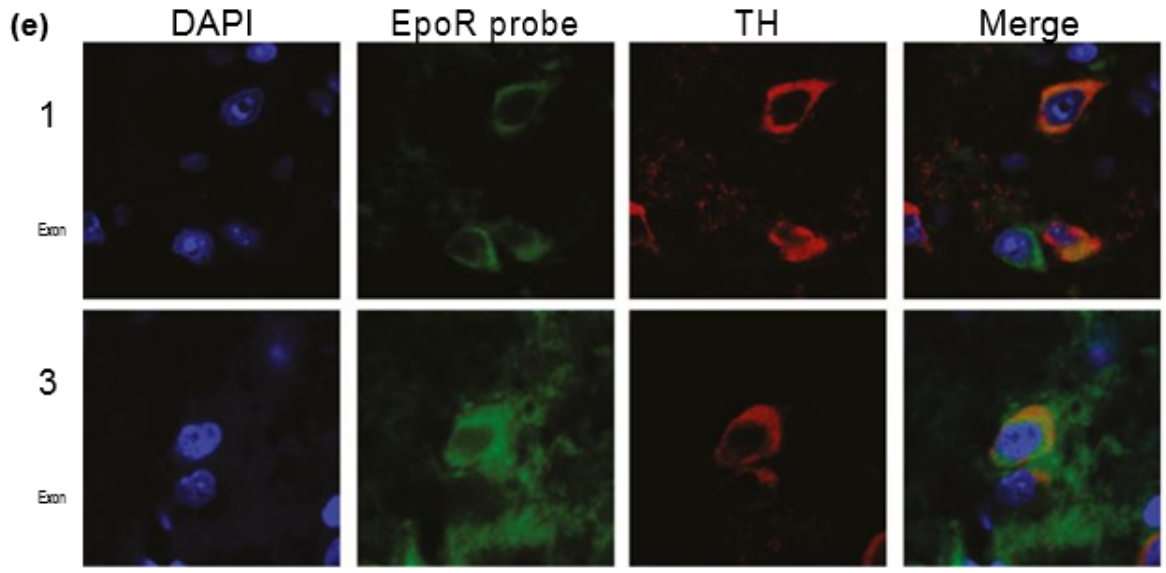

Fig. 2 Molecular anatomy of EpoR mRNAs. (a) 5′ rapid amplification of cDNA ends (RACE) validates the expression of DA-EpoR in isolated A9 neurons. Total RNA was prepared from spleen and from LMC-purified A9 DA neurons. Schematic representation of primers used for 5′ RACE and nested PCR and their position on EpoR exons are indicated on the right. PCR products from spleen and A9 cDNAs were analyzed on agarose gel. A negative control PCR reaction (NT) was also included. (b) Alternative EpoR variant is expressed in A9 and A10 neurons. RT-PCR was performed on RNA prepared from isolated A9 and A10 neurons, and from ventral midbrain (VM) and spleen. For PCR amplification, forward primers were designed on the first and second exon, as indicated. Reverse primer was placed on the third exon. Cellular purity was verified with primers targeting specific markers: Tyrosine hydroxylase (TH) for DA neurons (A9 and A10) and glial fibrillary acidic protein (GFAP) for astrocytes. (c) A9 neurons express DA-EpoR. Transcript anatomy was verified by PCR with exon-specific primers, as indicated in the scheme. cDNA from spleen and from LCM-purified A9 neurons was used for PCR reactions. (d) DA-EpoR and FL-EpoR have the same 3′ end. Total RNA was prepared from spleen and LCM-purified A9 neurons. 3′ RACE was performed with specific primers as indicated on the right. (e) EpoR exon1 and exon3-specific LNA probes decorate mDA neurons. Ventral midbrain slices were processed for in situ hybridization experiments. Specific LNA probes were designed to target exon 1 and exon 3, as indicated (green). DA neurons were visualized by immunohistochemistry with anti-TH antibody (red). Nuclei are in blue (DAPI). Representative images of staining in A9 neurons are shown.

To confirm 5′ RACE data, RT-PCR experiments were carried out with two different forward primers, one in the first exon and the latter in the second one coupled with a common reverse primer mapped on the third exon. As shown in Fig. 2b, EpoR gene was amplified starting from the first exon from spleen, whereas in A9 neurons, EpoR transcript was amplified when the forward primer located in the second exon was used. Interestingly, when we analyzed RNA purified from ventral midbrain after extensive perfusion with TBS, we found expression of FL-EpoR transcript.

RT-PCR was then carried out on the spleen and A9 DA neurons RNAs with a unique forward primer located in the first exon in combination with reverse primers that mapped to all the eight exons of the gene.

As shown in Fig. 2c, all these primer pairs were able to amplify EpoR transcripts when used on spleen cDNA. How-ever, they did not amplify any transcript from A9 DA cells. When a forward primer on the second exon was used, EpoR transcripts were detected in A9 cells for all primer combinations.

To elucidate the molecular anatomy of the 3′ end, we carried out 3′ RACE on RNA from spleen and 5000 A9 neurons harvested with LCM. The retrotranscription was performed with the GeneRacer™ OligodT Primer by taking advantage of forward primers mapping on the fifth exon. As shown in Fig. 2d, the size of the amplicons in the spleen and A9 showed no differences while cloning and sequencing confirmed the expected cDNAs.

A combination of in situ hybridization with anti-tyrosine hydroxylase immunofluorescence was then carried out on coronal sections of ventral midbrain of mouse adult brains. Two LNA probes were used for in situ hybridization: one was designed on the first exon, in order to detect only FL-EpoR; the second probe was designed on the third exon in order to detect all the transcripts encoding EpoR (Pan-EpoR). Extensive perfusion was performed to minimize blood contamination. Surprisingly, as shown in the Fig. 2e, LNA probes for exon 1 and exon 3 gave both specific and reproducible signals in A9 DA neurons as identified by anti-TH immunoreactivity and anatomical localization. Altogether, these data indicate that FL- and DA-EpoR mRNA isoforms are present in A9 DA neurons.

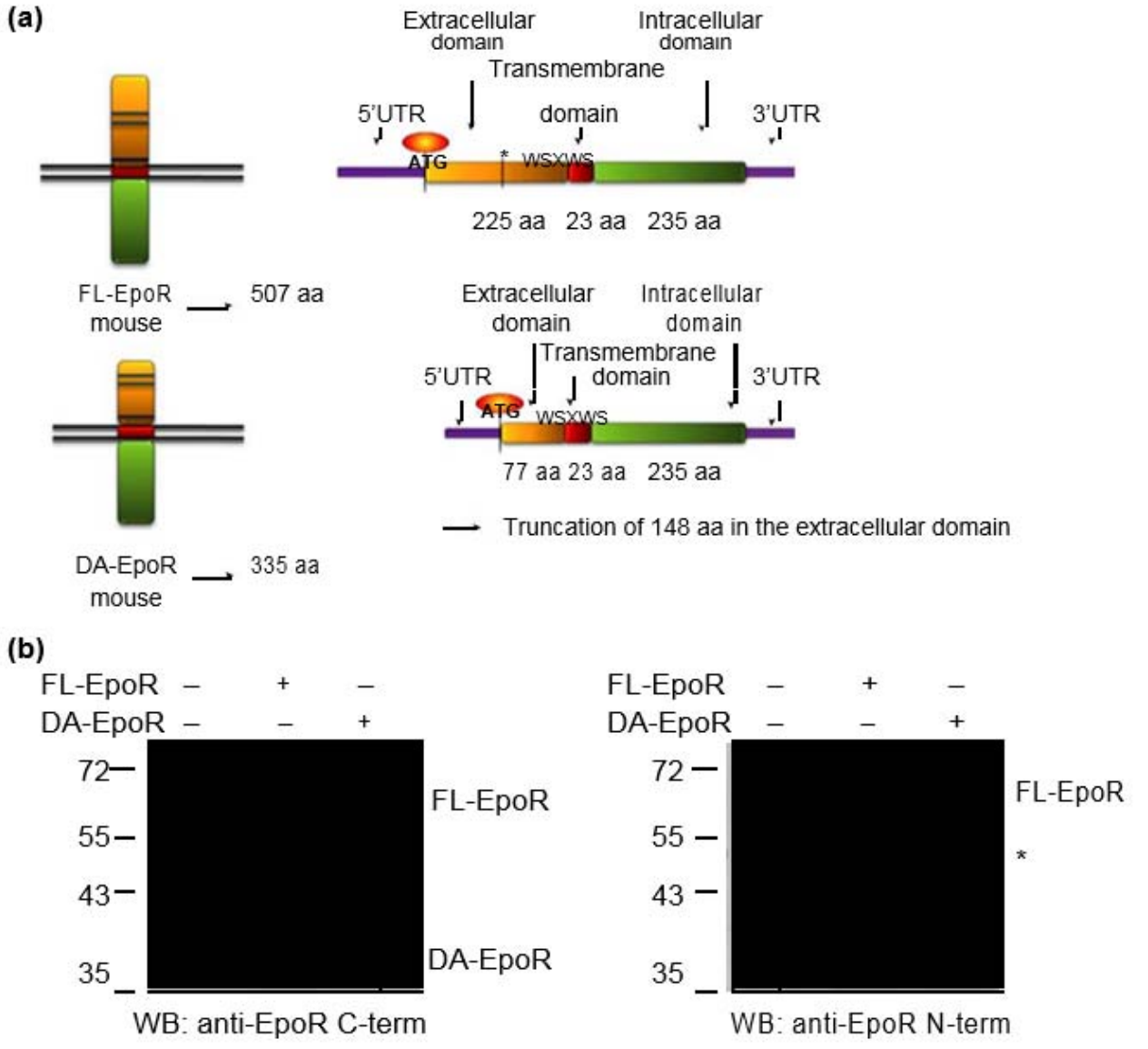

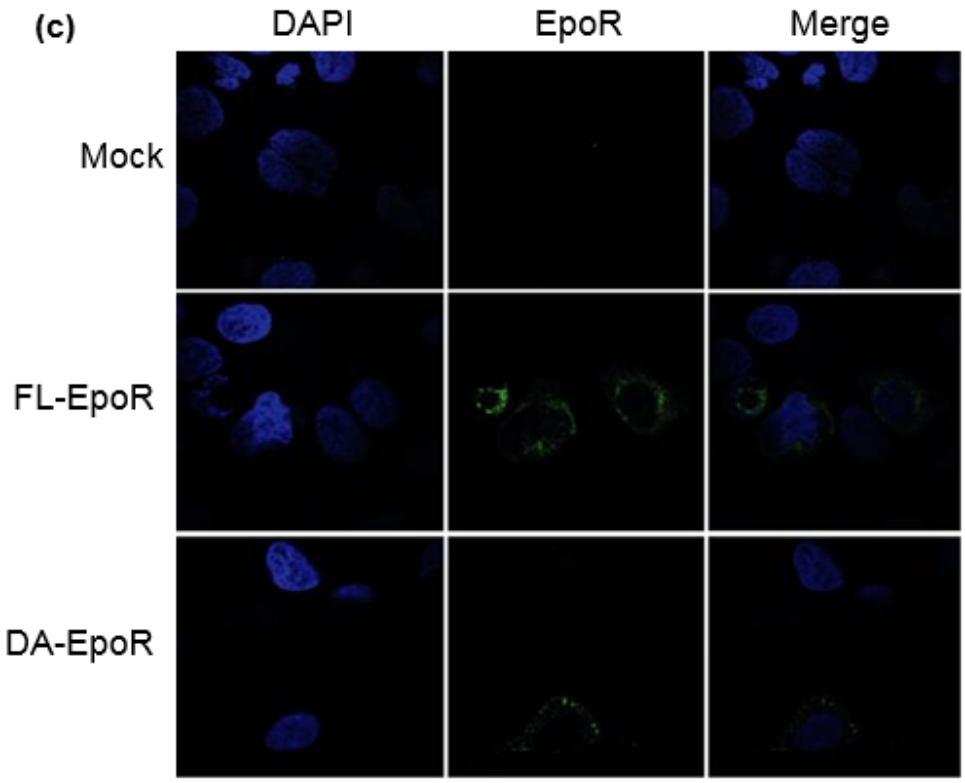

Fig. 3 Alternative TSS usage encodes for a N-terminal truncated EpoR. (a) Schematic representation of FL- and DA-EpoR. FL-and DA-EpoR proteins (left) and transcripts (right) are shown. EpoR functional domains are indicated: extracellular domain (yellow), transmembrane domain (red), and intracellular domain (green). Amino acid length for each domain is indicated at the bottom. (b) Expression of FL- and DA-EpoR. HEK 293T were transfected with pcDNA3 plasmids encoding for FL- and DA-EpoR or with an empty vector (control). Total lysates were analyzed by western blot with an anti-EpoR targeting the C-terminus (left) or the N-terminus (right) of the protein. Molecular weights are shown on the left. (c) Localization of FL- and DA-EpoR. Cells were transfected as in B. Anti-EpoR C-terminus and N-terminus specific antibodies were used for immunocytochemistry. EpoR signals are in green, nuclei in blue. Mock-transfected cells were used as control.

Protein expression analysis of DA-EpoR

FL-EpoR sequence has the first ATG in the first exon and produces a protein of 507 amino acids. Since the DA-EpoR isoform lacks this exon, by conceptual translation we identified an open reading frame of 335 amino acids starting from a methionine (Met) in the third exon. Interestingly, this Met corresponds to amino acid 149 of the full-length EpoR suggesting that DA-EpoR encodes for a N-terminal truncated variant that presents a shorter extracellular region while it maintains the transmembrane and cytoplasmic domains (Fig. 3a).

FL- and DA-EpoRs cDNAs were then introduced into the pcDNA3.1(-) expression vector and transfected into HEK 293T cells that lacks endogenous EpoR. To confirm the different N-terminal regions and shared C-ends, the anti-C-terminal part of EpoR M-20 was used in combination with the anti-EpoR W-20 directed against the first amino acids at the N-terminal, present exclusively in the FL-encoded form.

As shown in Fig. 3b, the anti-EpoR M-20 antibody recognized two EpoRs of different size: one of about 68 kDa and a smaller one of about 38 kDa. As expected, the antibody directed against the N-terminal part of EpoR

recognized only the FL-derived form, demonstrating that DA-EpoR lacks a part of its extracellular portion (Fig. 3b). These results were confirmed by immunofluorescence (Fig. 3c).

To assess if the truncated isoform of EpoR is expressed in a dopaminergic cell line in vitro, we took advantage of MN9D mouse dopaminergic cell line over-expressing Nurr-1 under a doxycycline-inducible promoter MN9D-Nurr1$^{Tet\text{-}On}$ (Hermanson et al. 2003). Nurr-1 is a key dopaminergic transcription factor required for late-dopaminergic differentiation. Upon its activation, many DA-specific genes are induced including the vesicular monoamine transporter 2 (VMAT2). Western blot analysis was performed on undifferentiated cells and after 96h from Nurr1 induction.

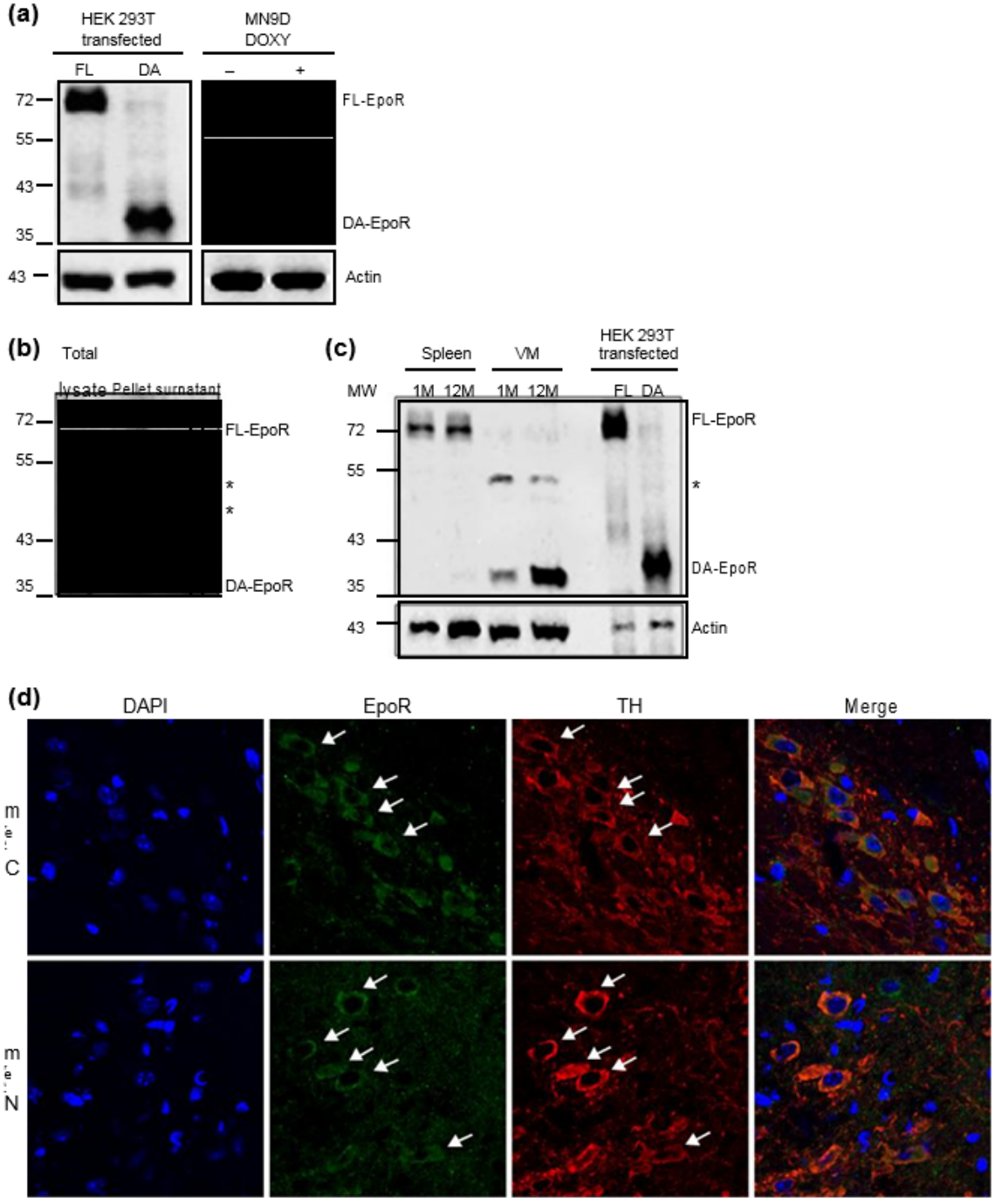

Fig. 4 Endogenous EpoR variants are expressed in dopaminergic cell line and in mouse brain. (a) Murine dopaminergic MN9D-Nurr1^{TetOn} cells were differentiated with doxycycline. Endogenous FL- and DA-EpoR variants were detected by western blot with anti-EpoR C-terminal specific antibody. b-actin was used as loading control. Western blot with lysates from HEK 293T cells transfected with FL- and DA-EpoR plasmids were used for reference of protein signals. (b) DA-EpoR is detected in the pellet fraction from mouse midbrain. Ventral midbrain was dissected from mouse brain after extensive perfusion with Tris-buffered saline (TBS). Total protein lysate was prepared and used to separate pellet and supernatant fractions. Proteins from each fraction were analyzed with anti-EpoR (C-terminal) antibody. Asterisks indicate unspecific bands. (c) Endogenous DA-EpoR is detected in the mouse brain of young and aged mice. Spleen and ventral midbrain were dissected from 1 month (1M) and 12 months (12M) mice and used to prepare protein lysates. Endogenous EpoR isoforms were detected using C-terminal-specific antibody, as in B. b-actin was used as loading control. Lysates from FL- and DA-EpoR transfected HEK 293T cells were used as positive controls. (d) Endogenous EpoR is detected by immunohistochemistry in DA neurons. Ventral midbrain slices were stained with anti-EpoR (green) using C-terminal-specific (upper panels) and N-terminal-specific (lower panels) antibodies. DA neurons were visualized with anti-TH antibody (red). Nuclei were stained with DAPI (blue). Examples of EpoR-expressing TH-positive neurons are indicated with white arrows.

As shown in Fig. 4a, these cells endogenously express both EpoR isoforms.

At protein levels, DA-EpoR expression is also detected in vivo from lysates prepared from mouse ventral midbrain (Fig. 4b). We then carried out membrane preparation from spleen and ventral midbrain of 1- and 12-month-old mice using the Qproteome Cell Compartment Kit (Qiagen) noticing that DA-EpoR expression increases from 1 to 12 months of age (Fig. 4c).

A double immunohistochemical analysis with anti-EpoR M-20 (N-terminal) or W-20 (C-terminal) was then performed in combination with an anti-TH antibody to identify A9 DA neurons. This experiment revealed that DA cells were positive for EpoR staining with both antibodies (Fig. 4d). As proved by Western blot this experiment revealed that in addition to the N-terminal truncated isoform, DA cells express the FL-encoded EpoR.

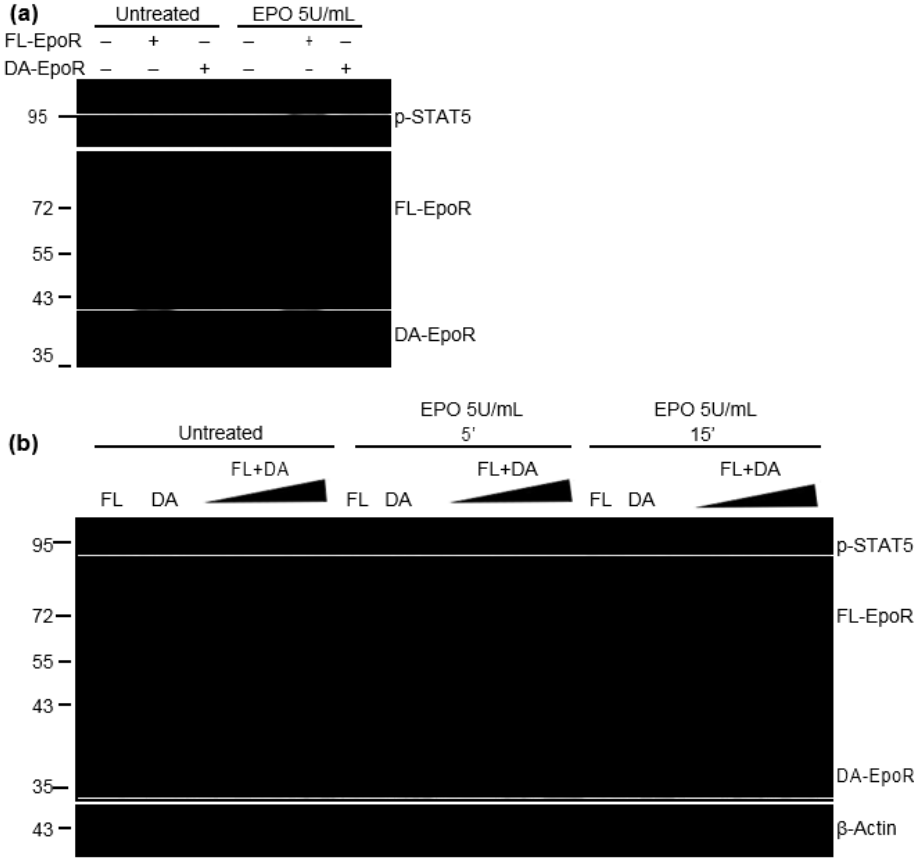

Fig. 5 DA-EpoR acts as decoy for erythropoietin (EPO)-mediated STAT5 phosphorylation. (a) DA-EpoR does not activate p-STAT5. HEK 293T cells were transfected with FL-EpoR or DA-EpoR, as indicated. Mock-transfected cells were used as controls. About 48 h after transfection, cells were treated with 5U/ml EPO for 15 minutes or left untreated. EPO-mediated EpoR activation was monitored by western blot using anti-phosphorylated STAT5 (p-STAT5) antibody. Expression of EpoR variants was checked with anti-EpoR C-terminal antibody. (b) Increasing doses of DA-EpoR plasmid were used to transfect HEK 293T cells in combination with FL-EpoR. Cells transfected with FL- or DA-EpoR alone were included as controls. After transfections, the cells were treated with 5U/ml EPO for 5 and 15 min. Control cells were left untreated. Activation of EPO/EpoR signaling was monitored by p-STAT5. Anti-EpoR C-terminal antibody was used to monitor the expression of EpoR variants. b-actin was included as loading control.

STAT5 phosphorylation assay

Since DA-EpoR is supposed to maintain EpoR binding, we monitor its activation by investigating the phosphorylation status of the transcription factor STAT5, EpoR major signal-ing target. After transfection with FL- or DA-EpoRs, HEK 293T cells were stimulated with 5 U/ml of recombinant human EPO for 15 min. As shown in Fig. 5a EPO treatment was able to trigger STAT5 phosphorylation in the presence of FL-EpoR but not when DA-EpoR was expressed. The failure to induce STAT5 phosphorylation was not because of insufficient amount of transfected DA-EpoR since increasing DA-EpoR quantity by inhibiting its degradation did not have any effects while transfecting 10-fold lower amount of FL-EpoR was sufficient to activate signaling (Fig. S1 and Fig. S2).

We then tested whether DA-EpoR may modulate FL-EpoR activity. For this purpose, we transfected HEK 293T cells with FL-EpoR or DA-EpoR alone, and with a combination of the two constructs, maintaining fixed FL-EpoR concentration while increasing DA isoform quantities. Cells were then treated with 5 U/mL EPO for $5'$ and for $15'$, and western blot was performed. As shown in Fig. 5b, when FL-EpoR is transfected in combination with the DA isoform, it failed to mediate STAT5 phosphorylation. This was specific for DA-EpoR since the over-expression of an unrelated protein, GFP, was not able to modify the ability of full-length EpoR to trigger STAT5 phosphorylation (Fig. S3).

Alternative EPOR in human SN

We then aimed to monitor the existence of alternative TSSs and their usage in human EPOR locus. We interrogated FANTOM5 hCAGE libraries from human cell lines, primary cells, and tissues for a total of 1829 samples (Arner et al. 2015; Forrest et al. 2014). Of those, 86 were derived from human brain samples and comprised primary cells (neurons, astrocytes, and Schwann cells) and selected brain areas from four independent donors.

Three different TSS regions can be identified using 'robust' decomposition-based peak identification method and referred to as p2/p3/p4, p8/p9, and p1, from $5'$ to $3'$ according to the sense of transcription (Fig. 6a). These drive expression of alternative variants of EPOR mRNA. TSS from p2/p3/p4 originates full-length mRNAs and is strongly used in CD34 precursor cells differentiated to erythrocyte lineage (160 TPM) and erythrocyte K562 cell line (30 TPM). p8/p9 is a weaker, erythrocyte-enriched promoter (7–10 TPM in differentiated erythrocytes). It is used in a restricted number of samples (14/1829 libraries), including mast cells. Unexpectedly, p1 represents the stronger promoter at EPOR locus, being expressed in 58% of the samples (1062/1829 libraries). Its TSS is located in intron 4. Its highest expression can be measured in white blood cells (macrophages, monocytes, T and NK cells), with values ranging from 10 to 60 TPM. Interestingly, samples with high levels of p1 transcript have low-no usage of p2/p3/p4, as shown for T-cell leukemia.

In the brain, the use of full-length and p1-derived EPOR transcript variant is mutually exclusive (Fig. 6a). All human brain-derived libraries (N = 82) express p1-derived EPOR and are completely devoid of full-length RNAs. Conversely, in red blood cells, where the FL isoform is predominant, p1-derived variant is virtually absent.

Interestingly, when comparing TSS usage in human SN with whole blood sample (Fig 6a, normalized scale), we noticed that SN shows the almost exclusive expression of p1-derived EpoR while in whole blood, instead, full-length and p1-derived EPOR transcript variants co-exist, possibly because of cellular composition of whole blood sample, which includes red and white cells.

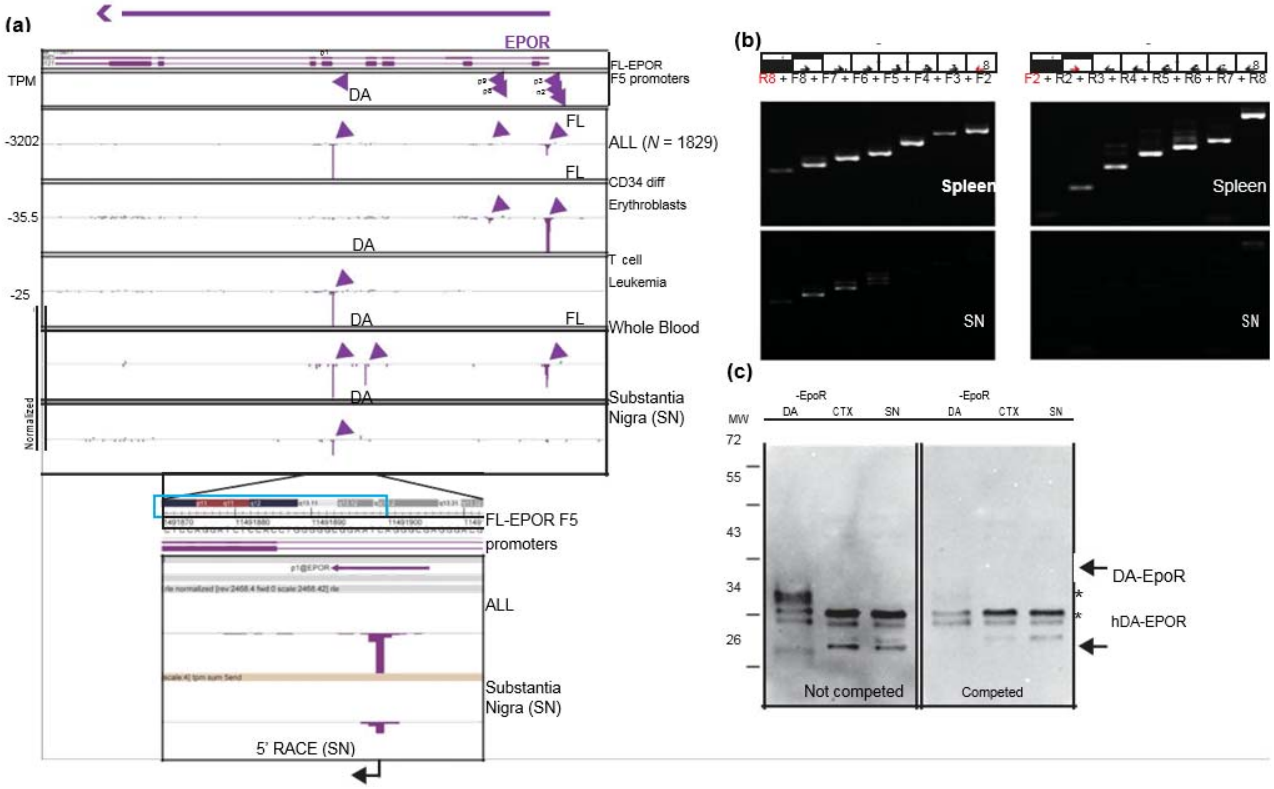

Fig. 6 Alternative EPOR in human SN. (a) Zenbu Genome Browser view of human EPOR locus. EpoR gene (purple arrow) and anatomy of full-length transcript are shown on top. Promoters identified with FANTOM5 decomposition-based peak identification method are shown (original promoter nomenclature is given): p2/p3/p4, p8/p9, and p1 are indicated in $5^{\prime}$ to $3^{\prime}$ direction. Tracks of hCAGE data are presented for all libraries pooled together (ALL, n = 1829) and for tissues/cells of interest, showing alternative transcription start site (TSS) usage (CD34 differentiation to erythroblasts, T-cell leukemia cells, whole blood, and SN). In each track, purple arrows highlight TSSs for EPOR variants identified by FANTOM5, including DA-EPOR. TSS supporting the expression of full-length Epor transcript in ALL, CD34 cells, and whole blood is also indicated. A zoomed-in image of the genomic region around the fourth intron or fifth exon boundary is provided, showing TSS usage in SN. A black arrow indicates the position of $5^{\prime}$ rapid amplification of cDNA ends (RACE) results from human SN post-mortem tissue sample. The validated sequence is highlighted by a blue box. (b) Expression of alternative EPOR variant in human SN. Transcript anatomy was verified by PCR with exon-specific primers, as indicated in the scheme. cDNA from spleen and SN was used for PCR reactions. (c) Human DA-EPOR can be detected in the human brain regions. Protein lysates were prepared from samples of human cortex and SN. Extract from mouse DA-EpoR transfected HEK 293T cells was loaded as positive control. Human DA-EPOR was detected with anti-EpoR-specific antibody (left panel). Signal specificity was checked by competition experiment (right panel). Asterisks indicate unspecific bands.

Validation of mRNA and protein expression of the human p1-derived EpoR variant

To validate the anatomy of the 5′ ends of EpoR mRNAs in human, we carried out a 5′ RACE experiment from spleen and SN post-mortem tissues. After ligation of a synthetic RNA oligonucleotide to the 5′ end of decapped RNA and retrotranscription, we used two different strategies to discriminate full-length EpoR from truncated EpoR forms. For full-length mRNA identification, RT-PCRs were carried out taking advantage of GeneRacer™ 5′ primers coupled to a reverse primer in the third exon and a nested one in the second. To study the truncated isoform, we resorted to a reverse primer in the seventh exon and a nested in the sixth exon (Fig. S4).

We thus found a major product (380 bp) in the spleen corresponding to full-length EpoR and a product of smaller size (320 bp) in the SN. Subcloning and sequencing of these fragments confirmed the existence of an alternative TSS from p1 present in the SN that lies about 642 bp 3′ to the canonical full-length 5′ end and it is localized in the fifth exon of the human EpoR gene (Fig. 6a and Fig. S4). As expected from FANTOM5 analysis, this truncated isoform is co-expressed with the full-length in the spleen, while it represents the major EpoR isoform in the SN.

RT-PCR was then carried out on human spleen and SN RNAs to validate the molecular anatomy of transcripts. As shown in Fig. 6b, while spleen was expressing FL-EPOR, in SN only, combinations of primers located in exons 5–8 were able to amplify a transcript.

The p1-derived transcript presents an open reading frame of 285 amino acids starting from a Met in the fifth exon. Interestingly, this Met corresponds to amino acid 200 of the full-length EpoR suggesting a similar organization as in mouse. The p1-derived EpoR encodes for a N-terminal truncated variant that presents a shorter extracellular region while it maintains the transmembrane and cytoplasmic domains.

Importantly, as shown in Fig. 6c, western blot from lysates prepared from post-mortem human SN and cortex proved the existence of this truncated form of EPOR in vivo. Detection specificity was verified by competition assay.

Discussion

The discovery that EPO/EpoR system exerts crucial non-hematopoietic functions has triggered a lot of interest in defining tissue-specific elements of this signaling path-way. This is particularly relevant to tailor EPO administration as therapeutic treatment for diseases of the nervous system.

While high-dose application of recombinant human EPO is the strategy of choice for treating acute conditions like stroke, long-term intervention for chronic neurodegenerative diseases eventually leads to several side-effects because of excessive stimulation of red blood cell production and consequent thromboembolic complications with potential lethality.

One strategy to overcome this important limitation is the synthesis of chemically modified forms of EPO that show preferential activation of signaling pathways in the brain. In this context, carbamylated EPO does not have erythropoietic activity while confers neuroprotective function in several animal models of diseases, including Alzheimer's disease and ischemic stroke (Armand-Ugon et al. 2015; Garcia-Rodriguez and Sosa-Teste 2009). Then, a fundamental question involves EpoR structure and the existence of cell-specific isoforms as potential targets for drug design. Activation of JAK/STAT and Ras/MAP pathways involves the homodimerization of FL-EpoR. EPO can also signal via a heterodimeric receptor composed of an EpoR monomer chain and CD131 (Brines and Cerami 2006; Zhang et al. 2009). The activation of this heterodimeric complex requires much higher concentrations of EPO and is found in non-erythroid cells (Hand and Brines 2011).

In this context, we are interested in the potential neuro-protective activity of EPO on mesencephalic A9 DA cells and its use as therapeutics for PD. A9 DA neurons of the SN form the mesostriatal system and are involved in regulating voluntary movements and postural reflexes. They express enzymatic pathways involved in

dopamine synthesis, release, and metabolism. They also present a spontaneous pacemaker activity when in the absence of synaptic inputs. A throughout transcriptional profiling of A9 neurons may provide fundamental information on their physiology and on the mechanisms of cell-type specific dysfunction in PD. By taking advantage of nanoCAGE and FANTOM5 hCAGE, we show mouse and human EpoR genes present alternative TSSs that give rise to N-terminal truncated EpoR. Importantly, we provide evidence that these are the main transcripts isoforms in non-hematopoietic tissues.

Several experimental data have been accumulated in support of the existence of these EpoR transcript variants. First, hCAGE and nanoCAGE show experimental evidence of TSSs. CAGE is the standard for promoter identification (Andersson et al. 2014; Arner et al. 2015; Forrest et al. 2014). NanoCAGE extends the ability to monitor genome-wide promoter usage to a homogenous population of a small number of purified cells (Plessy et al. 2010). The evidence of TSS variants on EpoR is supported by hCAGE experimental data on a very large collection of mouse and human samples in FANTOM5 and it is fitting perfectly nanoCAGE TSS distribution in A9 DA cells. We have then provided additional experimental support by taking advantage of $5^{/}$ RACE, RT-PCR, and expression cloning. Importantly, we have then shown that DA cells in vitro and in vivo express a truncated form of EpoR protein with a size and immunoreactivity compatible with the molecular anatomy of transcripts. However, in situ hybridization, immunocytochemistry, and western blot analysis prove that FL-EpoR mRNA and protein do exist in DA neurons in vitro and in vivo, while nanoCAGE and RT-PCR experiments on LCM-purified A9 cells failed to detect these transcripts. The biological and/or technical basis of these discrepancies remains unclear. Transcripts may contain different CAP structures and/or lengths of polyA tails that may favor or inhibit full-length cloning. Furthermore, differential harvest of subcellular compartments with LCM may lead to sampling of cell body- and dendritic-associated mRNAs. Further experiments are required to fully account for these differences.

Conceptual translation of mouse and human EpoRs suggests that they maintain the WSXWS EPO-binding domain in the residual extracellular region. We have extensively tested whether the transfection of DA-EpoR alone was sufficient to activate signaling. To this purpose, we have over-expressed DA-EpoR in HEK cells, added recom-binant EPO, and monitored its activity by assaying the phosphorylation status of STAT5, a well-known downstream target event of EPO-dependent pathways. While in these conditions, transfected FL-EpoR was able to trigger a response in an highly reproducible manner, DA-EpoR failed to do so. No activity was also observed when we used carbamylated EPO (data not shown). Importantly, we also repeated the same experiments by co-transfecting DA-EpoR with full-length CD131, a partner of FL-EpoR in non-hematopoietic systems. Again, no STAT5 phosphorylation was evidenced upon EPO administration (data not shown). On the contrary, co-transfection of FL-EpoR and DA-EpoR led to a strong, specific, and reproducible inhibition of EPO signaling.

Several open questions remain unanswered. First and foremost, DA-EpoR may be able to trigger a new signaling pathway that does not involve STAT5 activation. Recently, EPO has been shown to trigger a signaling cascade involving a serpin–lysosome–cathepsin axis that is required for the cytoprotective effects of EPO on maturing populations of erythroblasts (Dev et al. 2013). Given the role of autophagy in the well-being of A9 DA neurons and its dysfunction in PD, it will be interesting to assess whether these alternative pathways are indeed targeted by DA-EpoR activation. On the other hand, one may speculate that a still unidentified co-receptor may be needed for EPO signaling at DA-EpoR. Furthermore, it has been postulated that signaling may require components of the extracellular matrix or cell-to-cell communication as well as the co-application of additional cytokines. All these important questions leave open the possibility that DA-EpoR may activate FL-EpoR-independent signaling events in physiological conditions.

It is experimentally validated that at least in vitro DA-EpoR acts as a decoy for EPO/FL-EpoR system. Given the well-established role of EPO signaling in A9 DA neurons as well as in non-hematopoietic cells, these results indicate that cells must express a heterogeneous repertory of EpoRs suggesting a previously unnoticed level of regulation. Intriguingly, we have found that the ratio between FL-EpoR and DA-EpoR in SN changes during lifetime in mice suggesting a potential mechanism for a decrease of neuro-protective activity of endogenous EPO in the aging brain.

In summary, we have provided evidence of the presence of EpoR isoforms in non-hematopoietic tissues that may help the rational design of a new group of drugs acting at this crucial signaling system and avoiding the unwanted detrimental effects on ectopic proliferation of erythroblasts.

Acknowledgments and conflict of interest disclosure

We are indebted to all the members of the SG lab for thought-provoking discussions and to Cristina Leonesi for technical support. We thank Prof. Ferrer (Institute of Neuropathology, IDIBELL-University Hospital of Bellvitge, Spain) for kindly providing CEPO. This work was funded by Ministero dell'Istruzione, dell'Universita e della Ricerca, (Grant/Award Number: FIRB (RBAP11FRE9)) to S.G., European Commission (Grant/Award Number: FP7-HEALTH DOPAMINET (223744)) to S.G. and P.C., and Ministry of Education, Culture, Sports, Science, and Technology (MEXT) to P.C. The authors declare that they have no conflicts of interest with the contents of this article.

All experiments were conducted in compliance with the ARRIVE guidelines.

Supporting information

Additional Supporting Information may be found online in the supporting information tab for this article:

Figure S1. FL-EpoR can signal even when expressed at low doses.

Figure S2. DA-EpoR stimulation upon proteasome inhibition.

Figure S3. Specificity of DA-EpoR decoy activity.

Figure S4. Characterization of human EpoR transcripts by $5^{\prime}$ RACE PCR analysis.

References

Andersson R., Gebhard C., Miguel-Escalada I., et al. (2014) An atlas of active enhancers across human cell types and tissues. Nature 507, 455–461.

Armand-Ugon M., Aso E., Moreno J., Riera-Codina M., Sanchez A., Vegas E. and Ferrer I. (2015) Memory improvement in the AbetaPP/PS1 mouse model of familial Alzheimer's disease induced by carbamylated-erythropoietin is accompanied by modulation of synaptic genes. J. Alzheimer's Dis. 45, 407–421.

Arner E., Daub C. O., Vitting-Seerup K., et al. (2015) Gene regulation. Transcribed enhancers lead waves of coordinated transcription in transitioning mammalian cells. Science 347, 1010–1014.

Bazan J. F. (1989) A novel family of growth factor receptors: a common binding domain in the growth hormone, prolactin, erythropoietin and IL-6 receptors, and the p75 IL-2 receptor beta-chain. Biochem. Biophys. Res. Commun. 164, 788–795.

Biagioli M., Pinto M., Cesselli D., et al. (2009) Unexpected expression of alpha- and beta-globin in mesencephalic dopaminergic neurons and glial cells. Proc. Natl Acad. Sci. USA 106, 15454–15459.

Brines M. and Cerami A. (2006) Discovering erythropoietin's extra-hematopoietic functions: biology and clinical promise. Kidney Int. 70, 246–250.

Brines M. L., Ghezzi P., Keenan S., Agnello D., de Lanerolle N. C., Cerami C., Itri L. M. and Cerami A. (2000) Erythropoietin crosses the blood-brain barrier to protect against experimental brain injury. Proc. Natl Acad. Sci. USA 97, 10526–10531.

Carninci P., Sandelin A., Lenhard B., et al. (2006) Genome-wide analysis of mammalian promoter architecture and evolution. Nat. Genet. 38, 626–635.

Carrieri C., Cimatti L., Biagioli M., et al. (2012) Long non-coding antisense RNA controls Uchl1 translation through an embedded SINEB2 repeat. Nature 491, 454–457.

Carrieri C., Forrest A. R., Santoro C., Persichetti F., Carninci P., Zucchelli S. and Gustincich S. (2015) Expression analysis of the long non-coding RNA antisense to Uchl1 (AS Uchl1) during dopaminergic cells' differentiation in vitro and in neurochemical models of Parkinson's disease. Front. Cellular Neurosci. 9, 114.

Chong Z. Z., Kang J. Q. and Maiese K. (2003) Erythropoietin fosters both intrinsic and extrinsic neuronal protection through modulation of microglia, Akt1, Bad, and caspase-mediated pathways. Br. J. Pharmacol. 138, 1107–1118.

Constantinescu S. N., Ghaffari S. and Lodish H. F. (1999) The erythropoietin receptor: structure, activation and intracellular signal transduction. Trends Endocrinol. Metab. 10, 18–23.

Dame C., Juul S. E. and Christensen R. D. (2001) The biology of erythropoietin in the central nervous system and its neurotrophic and neuroprotective potential. Biol. Neonate 79, 228–235.

Dev A., Byrne S. M., Verma R., Ashton-Rickardt P. G. and Wojchowski D. M. (2013) Erythropoietin-directed erythropoiesis depends on serpin inhibition of erythroblast lysosomal cathepsins. J. Exp. Med. 210, 225–232.

Digicaylioglu M. and Lipton S. A. (2001) Erythropoietin-mediated neuroprotection involves cross-talk between Jak2 and NF-kappaB signalling cascades. Nature 412, 641–647.

Digicaylioglu M., Bichet S., Marti H. H., Wenger R. H., Rivas L. A., Bauer C. and Gassmann M. (1995) Localization of specific erythropoietin binding sites in defined areas of the mouse brain. Proc. Natl Acad. Sci. USA 92, 3717–3720.

Erbas O., Cinar B. P., Solmaz V., Cavusoglu T. and Ates U. (2015) The neuroprotective effect of erythropoietin on experimental Parkinson model in rats. Neuropeptides 49, 1–5.

Forrest A. R., Kawaji H., Rehli M., et al. (2014) A promoter-level mammalian expression atlas. Nature 507, 462–470.

Ganser C., Papazoglou A., Just L. and Nikkhah G. (2010) Neuroprotective effects of erythropoietin on 6-hydroxydopamine-treated ventral mesencephalic dopamine-rich cultures. Exp. Cell Res. 316, 737–746.

Garcia-Rodriguez J. C. and Sosa-Teste I. (2009) The nasal route as a potential pathway for delivery of erythropoietin in the treatment of acute ischemic stroke in humans. TheScientificWorldJournal 9, 970–981.

Grison A., Zucchelli S., Urzi A., et al. (2014) Mesencephalic dopaminergic neurons express a repertoire of olfactory receptors and respond to odorant-like molecules. BMC Genom. 15, 729.

Gustincich S., Batalov S., Beisel K. W., et al. (2003) Analysis of the mouse transcriptome for genes involved in the function of the nervous system. Genome Res. 13, 1395–1401.

Hand C. C. and Brines M. (2011) Promises and pitfalls in erythopoietin-mediated tissue protection: are nonerythropoietic derivatives a way forward? J. Investig. Med. 59, 1073–1082.

Hermanson E., Joseph B., Castro D., et al. (2003) Nurr1 regulates dopamine synthesis and storage in MN9D dopamine cells. Exp. Cell Res. 288, 324–334.

Jang W., Park J., Shin K. J., et al. (2014) Safety and efficacy of recombinant human erythropoietin treatment of non-motor symptoms in Parkinson's disease. J. Neurol. Sci. 337, 47–54.

Jia Y., Mo S. J., Feng Q. Q., Zhan M. L., OuYang L. S., Chen J. C., Ma Y. X., Wu J. J. and Lei W. L. (2014) EPO-dependent activation of PI3K/Akt/FoxO3a signalling mediates neuroprotection in in vitro and in vivo models of Parkinson's disease. J. Mol. Neurosci. 53, 117–124.

Juul S. E., Anderson D. K., Li Y. and Christensen R. D. (1998) Erythropoietin and erythropoietin receptor in the developing human central nervous system. Pediatr. Res. 43, 40–49.

Kawakami M., Sekiguchi M., Sato K., Kozaki S. and Takahashi M. (2001) Erythropoietin receptor-mediated inhibition of exocytotic glutamate release confers neuroprotection during chemical ischemia. J. Biol. Chem. 276, 39469–39475.

Klingmuller U., Lorenz U., Cantley L. C., Neel B. G. and Lodish H. F. (1995) Specific recruitment of SH-PTP1 to the erythropoietin receptor causes inactivation of JAK2 and termination of proliferative signals. Cell 80, 729–738.

Lee J. Y., Koh H. C., Chang M. Y., Park C. H., Lee Y. S. and Lee S. H. (2003) Erythropoietin and bone morphogenetic protein 7 mediate ascorbate-induced dopaminergic differentiation from embryonic mesencephalic precursors. NeuroReport 14, 1401–1404.

Livnah O., Stura E. A., Johnson D. L., Middleton S. A., Mulcahy L. S., Wrighton N. C., Dower W. J., Jolliffe L. K. and Wilson I. A. (1996) Functional mimicry of a protein hormone by a peptide agonist: the EPO receptor complex at 2.8 A. Science 273, 464–471.

Marti H. H., Wenger R. H., Rivas L. A., Straumann U., Digicaylioglu M., Henn V., Yonekawa Y., Bauer C. and Gassmann M. (1996) Erythropoietin gene expression in human, monkey and murine brain. Eur. J. Neuorsci. 8, 666–676.

Masuda S., Okano M., Yamagishi K., Nagao M., Ueda M. and Sasaki R. (1994) A novel site of erythropoietin production. Oxygen-dependent production in cultured rat astrocytes. J. Biol. Chem. 269, 19488–19493.

Matsushita N., Okada H., Yasoshima Y., Takahashi K., Kiuchi K. and Kobayashi K. (2002) Dynamics of tyrosine hydroxylase promoter activity during midbrain dopaminergic neuron development. J. Neurochem. 82, 295–304.

Merelli A., Czornyj L. and Lazarowski A. (2015) Erythropoietin as a new therapeutic opportunity in brain inflammation and neurodegenerative diseases. Int. J. Neurosci. 125(11), 793–797.

Obernosterer G., Martinez J. and Alenius M. (2007) Locked nucleic acid-based in situ detection of microRNAs in mouse tissue sections. Nat. Protoc. 2, 1508–1514.

Pedroso I., Bringas M. L., Aguiar A., Morales L., Alvarez M., Valdes P. A. and Alvarez L. (2012) Use of Cuban recombinant human erythropoietin in Parkinson's disease treatment. MEDICC Rev. 14, 11–17.

Plessy C., Bertin N., Takahashi H., et al. (2010) Linking promoters to functional transcripts in small samples with nanoCAGE and CAGEscan. Nat. Methods 7, 528–534.

Plessy C., Pascarella G., Bertin N., et al. (2012) Promoter architecture of mouse olfactory receptor genes. Genome Res. 22, 486–497.

Qi C., Xu M., Gan J., Yang X., Wu N., Song L., Yuan W. and Liu Z. (2014) Erythropoietin improves neurobehavior by reducing dopaminergic neuron loss in a 6-hydroxydopamine-induced rat model. Int. J. Mol. Med. 34, 440–450.

Schneider H., Chaovapong W., Matthews D. J., et al. (1997) Homodimerization of erythropoietin receptor by a bivalent monoclonal antibody triggers cell proliferation and differentiation of erythroid precursors. Blood 89, 473–482.

Severin J., Lizio M., Harshbarger J., Kawaji H., Daub C. O., Hayashizaki Y., Bertin N. and Forrest A. R. (2014) Interactive visualization and analysis of large-scale sequencing datasets using ZENBU. Nat. Biotechnol. 32, 217–219.

Shiraki T., Kondo S., Katayama S., et al. (2003) Cap analysis gene expression for high-throughput analysis of transcriptional starting point and identification of promoter usage. Proc. Natl Acad. Sci. USA 100, 15776–15781.

Signore A. P., Weng Z., Hastings T., Van Laar A. D., Liang Q., Lee Y. J. and Chen J. (2006) Erythropoietin protects against 6-hydroxydopamine-induced dopaminergic cell death. J. Neurochem. 96, 428–443.

Siren A. L., Knerlich F., Poser W., Gleiter C. H., Bruck W. and Ehrenreich H. (2001) Erythropoietin and erythropoietin receptor in human ischemic/hypoxic brain. Acta Neuropathol. 101, 271–276.

Tsai P. T., Ohab J. J., Kertesz N., Groszer M., Matter C., Gao J., Liu X., Wu H. and Carmichael S. T. (2006) A critical role of erythropoietin receptor in neurogenesis and post-stroke recovery. J. Neurosci. 26, 1269–1274.

Vogel J. and Gassmann M. (2011) Erythropoietic and non-erythropoietic functions of erythropoietin in mouse models. J. Physiol. 589, 1259–1264.

Witthuhn B. A., Quelle F. W., Silvennoinen O., Yi T., Tang B., Miura O. and Ihle J. N. (1993) JAK2 associates with the erythropoietin receptor and is tyrosine phosphorylated and activated following stimulation with erythropoietin. Cell 74, 227–236.

Xue Y. Q., Zhao L. R., Guo W. P. and Duan W. M. (2007) Intrastriatal administration of erythropoietin protects dopaminergic neurons and improves neurobehavioral outcome in a rat model of Parkinson's disease. Neuroscience 146, 1245–1258.

Xue Y. Q., Ma B. F., Zhao L. R., Tatom J. B., Li B., Jiang L. X., Klein R. L. and Duan W. M. (2010) AAV9-mediated erythropoietin gene delivery into the brain protects nigral dopaminergic neurons in a rat model of Parkinson's disease. Gene Ther. 17, 83–94.

Yamamoto M., Koshimura K., Kawaguchi M., Sohmiya M., Murakami Y. and Kato Y. (2000) Stimulating effect of erythropoietin on the release of dopamine and acetylcholine from the rat brain slice. Neurosci. Lett. 292, 131–133.

Yu X., Lin C. S., Costantini F. and Noguchi C. T. (2001) The human erythropoietin receptor gene rescues erythropoiesis and developmental defects in the erythropoietin receptor null mouse. Blood 98, 475–477.

Zhang Y. L., Radhakrishnan M. L., Lu X., Gross A. W., Tidor B. and Lodish H. F. (2009) Symmetric signaling by an asymmetric 1 erythropoietin: 2 erythropoietin receptor complex. Mol. Cell 33, 266–274.